Journal of Ambient Intelligence and Humanized Computing
https://doi.org/10.1007/s12652-020-02430-z

ORIGINAL RESEARCH

Scintillation and bit error rate calculation of Mathieu–Gauss beam in turbulence

Mert Bayraktar[1]

Received: 21 February 2020 / Accepted: 25 July 2020

Abstract
We present on-axis, aperture averaged scintillation, and bit error rate performance of Mathieu–Gauss beams (MGB). We model atmosphere utilizing random phase screen. Our investigations show that scintillation indexes of both odd and even modes of MGBs are less than Gauss beam. In the comparison of odd and even modes, odd modes draw the attention with its less scintillation index. In case of aperture averaged scintillation, all types of MGBs are advantageous comparing with Gauss beam but this advantage vanishes with increase in receiver aperture opening. Mitigation in scintillation index brings us 10^{-6} times lesser bit error rate (BER) than Gauss beam.

Keywords Mathieu–Gauss beam · Scintillation · Bit error rate · Atmospheric turbulence · Aperture averaging

1 Introduction

Beam shaping has been one of the interesting topic for several years. Aim of beam shaping is to generate beams having different source field distribution than Gauss beam. Regarding with this phenomena, scientist introduced Bessel beam to scientific world in Durnin et al. (1987) indicating its non-diffracting property. Authors found one of the family members of Bessel beam: Mathieu beams in Gutiérrez-Vega et al. (2000). Formulation of this type of beam is given first time in (Gutierrez-Vega et al. 2000) starting from McCutchen sphere. Scientists introduce a parabolic beam in Bandres et al. (2004) and they investigate that found beam can be described via Mathieu beams. After invention of MGB, zero order one is generated first time experimentally (Gutierrez-Vega et al. 2001). Changing symmetry of axicon cavity, it is possible to generate MGB in desired order (Alvarez-Elizondo et al. 2008). In the generation of vector Mathieu-like hollow beam, authors in Li and Yin (2011) benefit from axicon and dual mode elliptic hollow fiber. This study shows that generated beam has orbital angular momentum and it protects this property up to 2.2 m distance. In addition to axicon, scientists use amplitude modulation type spatial light modulator(SLM) to generate Mathieu beams (Ren et al. 2018). It is shown in Hernandez–Hernandez et al. (2010) that even, odd, and helical modes of MGB can be generated using phase only SLM. Minimum number of Bessel-Gauss beams is determined to generate MGB in Gutierrez-Vega and Bandres (2007). Adjusting ellipticity parameter, it is possible apply OAM according to Lopez-Mariscal et al. (2006). It is mentioned in Barcelo-Chong et al. (2018) that asymmetric Mathieu beams can be generated adjusting ellipticity, asymmetry parameters, and angular position. In Chafiq et al. (2006), authors indicate that intensity profile of MGB is similar with Bessel-Gauss beam after propagation through ABCD optical systems. Propagation of MGB through paraxial optical system is studied (Hernandez-Aranda et al. 2006) and through atmosphere utilizing Rytov theory in Noriega-Manez and Gutierrez-Vega (2007).

Turbulence is the irregular air movements which occurs because of sudden temperature and pressure changes. Bearing in mind this, propagation of a beam through the atmosphere can be analyzed applying two methods. Solution of Huygens-Fresnel integral gives received analytically (Andrews 2005). Random phase screen(RPS) approach is another way to evaluate received field numerically (Schmidt 2010).

Irradiance fluctuations of laser beam through turbulent atmosphere is defined by Fried and Seidman (1967). Additionally, scintillation expression for Gauss beam is derived

✉ Mert Bayraktar
mert.bayraktar@hku.edu.tr

[1] Department of Electric Electronic Engineering, Hasan Kalyoncu University, Havaalanı Yolu 8. km, Şahinbey, 27410 Gaziantep, Turkey

Published online: 31 July 2020

in Andrews et al. (2001). Studies in this aspect include analytical derivation or applying random phase screen approach to non-conventional beam types. In analytical point of view, it is investigated in Eyyuboglu (2013c) that scintillation index of airy beam is less than Gauss beam. It is showed in (Yao 2009) that astigmatic annular beams also have less scintillation index than Gauss beam. Another studies Öztan and Baykal (2010) and Baykal et al. (2008) indicate that asymmetry brings the advantage in case of point like scintillation. It is also possible to find scintillation index utilizing semi-analytic method as it is done in Eyyuboglu (2015b). Authors show that partially coherent beams have less scintillation for equal power case. Applying random phase screen approach, it is resulted (Eyyuboglu 2013b) that scintillation index of hypergeometric Gaussian beam decreases while hollowness parameter decreases for large Gaussian source sizes. Advantage of annular beam rather than sinusoidal and hyperbolic Gaussian beam is proved in Eyyuboglu (2013a). Annular Gauss and dark hollow beams bring the advantage as it is demonstrated in Eyyuboglu (2015a). It is presented in Bayraktar (2019) that it is possible to reduce point like scintillation increasing the order of sine hollow beam. Scintillation index reduces if source coherency reduces according to Qian et al. (2009). Dominancy of scintillation noise variance comparing with shot and thermal noise variances is showed in Eyyuboglu and Bayraktar (2015). Similarly, effect of underwater turbulence is tested via transmitting video (Priyalakshmi and Mahalakshmi 2020). On the other hand, possible data rates can reach up to 3.84 Tbps with distance 58,000 km since there is no turbulence between satellites (Sumathi et al. 2020).

Bit error rate or probability of error is used to measure the performance of a communication system. Based upon this phenomena, it is explained in Gercekcioglu and Baykal (2014) that increase in source size brings us reduction in BER. Coherence length of partially coherent flat-topped vortex hollow beam is decreased to obtain low BER as it is mentioned in Zhang et al. (2017). Annular beam shows better performance in terms of BER as compared to Gaussian beam (Gerçekçioğlu et al. 2010). Annular beam seems advantageous when small focal length and small beam size is used (Gercekcioglu and Baykal 2013). Cos-Gaussian beam can be used in optical wireless communication links for short distances since it brings us low BER (Arpali et al. 2008).

In this article, we study on-axis (point like) scintillation of Mathieu–Gauss beams utilizing random phase screen approach since received field and scintillation expressions of this type of beam hard to evaluate. In addition to on-axis scintillation, we show scintillation reduction while receiver aperture opening increases. Bearing in mind variance of on-axis scintillation, we compute BER value. All results are compared with Gauss beam because laser sources radiate in Gaussian distribution.

2 Numerical model for atmospheric turbulence

Source field expression Mathieu–Gauss beam in cylindrical coordinates is written form (Chafiq et al. 2006) as

$$
\begin{aligned}
&u_{es_{2n}}(s,\phi_s,q,z=0)\\
&\quad=\sum_{m=0}^{\infty}A_{2m}^{(2n)}q(-1)^{\mathrm{m}}\cos(2m\phi_s)J_{2m}(k_t s)\exp\left(-\frac{s^2}{\alpha_s^2}\right)\\
&u_{es_{2n+1}}(s,\phi_s,q,z=0)\\
&\quad=\sum_{m=0}^{\infty}A_{2m+1}^{(2n+1)}q(j)^{2\mathrm{m}+1}\cos[(2m+1)\phi_s]J_{2m+1}(k_t s)\exp\left(-\frac{s^2}{\alpha_s^2}\right)\\
&u_{os_{2n+2}}(s,\phi_s,q,z=0)\\
&\quad=\sum_{m=0}^{\infty}A_{2m+2}^{(2n+2)}q(-1)^{\mathrm{m}+1}\sin[(2m+2)\phi_s]J_{2m+2}(k_t s)\exp\left(-\frac{s^2}{\alpha_s^2}\right)\\
&u_{os_{2n+1}}(s,\phi_s,q,z=0)\\
&\quad=\sum_{m=0}^{\infty}A_{2m+1}^{(2n+1)}q(j)^{2\mathrm{m}+1}\sin[(2m+1)\phi_s]J_{2m+1}(k_t s)\exp\left(-\frac{s^2}{\alpha_s^2}\right)
\end{aligned}
\tag{1}
$$

where u_{os} and u_{es} are odd and even modes, α_s refers to Gaussian source size, A_k^l constant is defined in Gradshteyn and Ryzhik (2015), k_t is being the transverse coordinate the wave vector, ellipticity parameter $q=h^2k_t^2/4$ with $2h$ refers to distance between focal lengths of lenses in lens system, J_n is the nth order Bessel function, and $j=\sqrt{-1}$. As it is seen from Eq. (1), source field expression of MGB is composed of summation of Bessel function, trigonometric identity, and Gauss exponential product. Received field after propagation is written as

$$
u_r(\mathbf{r},L)=u_r\left(r_x,r_y,L\right)=\exp\left(jkL\right)\prod_{\mathbf{i}=\mathbf{1}}^{N_s}\mathbf{F}^{-\mathbf{1}}\left(\begin{array}{c}\mathbf{F}\left[u_{r_i}\left(s_{xi},s_{yi},iL_{\mathrm{i}}\right)\exp\left(j\phi_i\right)\right]x\\ \mathbf{F}\left\{\frac{-\mathrm{jk}}{2\pi L_{\mathrm{i}}}\exp\left(\frac{\mathrm{jk}}{2L_{\mathrm{i}}}\left[\left(r_{xi}-s_{xi}\right)^2+\left(r_{yi}-s_{yi}\right)^2\right]\right)\right\}\end{array}\right)
\tag{2}
$$

where $u_{r_i}\left(s_{xi}, s_{yi}, iL_i\right) = u_s\left(s_x, s_y, 0\right)$ as an initial case $\left(s_{xi}, s_{yi}\right)$ are input transverse plane coordinates of i th screen which corresponds to receiver transverse plane coordinates $r_{x_{i-1}}, r_{y_{i-1}}$, ϕ_i refers to random phase of i th screen and L_i is the distance between each screen. Scintillation measures the amount of intensity fluctuations and well-known scintillation index formula is written as

$$m_p^2 = \frac{\frac{1}{N}\sum_{i=1}^{N}\left[I_r(\mathbf{r},\ L)\right]^2}{\left[\frac{1}{N}\sum_{i=1}^{N}\left[I_r(\mathbf{r},\ L)\right]\right]^2} - 1 \tag{3}$$

where received intensity is being $I_r(\mathbf{r},\ L) = u_r(\mathbf{r},\ L)u_r^*(\mathbf{r},\ L)$ and * denoting complex conjugate. Bit error rate which is used to measure the communication link performance is written in Bayraktar (2019) as

$$BER = \frac{1}{2}\int_0^{\infty} p(x)\mathrm{erfc}\left(\frac{\langle \mathrm{SNR}\rangle x}{2\sqrt{2}}\right)dx \tag{4}$$

where erfc denotes the complementary error function and $p(x)$ refers to probability density function of scintillation index. For weak turbulent regime $p(x)$ is written as in Andrews and Philips (2004)

$$p(x) = \frac{1}{xAPm_p\left[\frac{1}{N}\sum_{i=1}^{N} I_r(\mathbf{r}, L)\right]\sqrt{2\pi}} \exp\left(-\frac{\left(\ln x + 0.5A^2P^2m_p^2\left[\frac{1}{N}\sum_{i=1}^{N} I_r(\mathbf{r}, L)\right]^2\right)^2}{2A^2P^2m_p^2\left[\frac{1}{N}\sum_{i=1}^{N} I_r(\mathbf{r}, L)\right]^2}\right) \tag{5}$$

In Eq. (5), A refers to magnification factor taken as 50 and $P = 0.5$ is the responsivity of photodiode. These values for A and P are selected like above because they are the average for commercial photodiodes. We use log-normal probability density function, since distribution of irradiance becomes log-normal under Rytov's first order approximation. Since, it is valid for weak and moderate turbulence regimes, our BER results are pertinent for these atmospheric conditions.

We set all beams to the same source dimensions 10 cm × 10 cm with equal 1 W power. Transverse plane is represented with 512 × 512 matrix notation. After determining the parameters, we choose source beam settings considering variations on k_t and α_s. RPS applications in literature are generally valid for weak and moderate turbulence conditions. According to Rao (2008), RPS can cover strong turbulent regime if number of screen increases. Bearing in mind this, we modify RPS and place 21, 51, and 91 randomly generated phase screens up to the distances in order 0–1200 m, 1200–3200 m, and 3200–5600 m as it is shown in Fig. 1. Number of screens are increased since cumulative turbulence should be less than Rytov index (Bayraktar and Eyyuboglu 2019). This way, random phase screen satisfies strong turbulence conditions. Screens are generated utilizing modified von-Karman power spectral density (PSD), because this PSD covers both inner and outer scale of atmosphere. Furthermore, modified von-Karman gives closer result to Hill spectrum (Andrews 2005). In our numerical set-up inner scale length is set as zero and outer scale length is set to infinity. Maximum Rytov number is used as 0.1 to limit maximum turbulence between hopes. In addition, turbulence strength is determined benefiting from refractive index structure constant C_n^2. $C_n^2 \in [10^{-14}, 10^{-12}]$ from weak to strong turbulence. These values are evaluated considering temperature, pressure and refractive index thermal constant. To measure on-axis scintillation, we set receiver plane coordinates 6 × 6

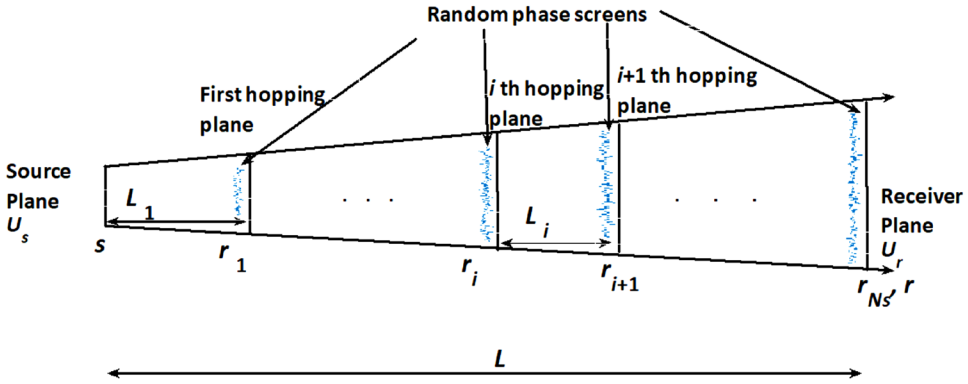

Fig. 1 Random phase screen model

which satisfy the point like scintillation condition which is mentioned in Eyyuboglu (2013a). In case of aperture averaged scintillation, receiver aperture grid size is increased and scintillation is evaluated via new form of Eq. (**3**)

$$m_A^2 = \frac{\frac{1}{N}\int dS \sum_{i=1}^{N}\left[I_r(\mathbf{r},\ L)\right]^2}{\int dS\left[\frac{1}{N}\sum_{i=1}^{N} I_r(\mathbf{r},\ L)\right]^2} - 1 = \frac{\left\langle P(r,\ L)^2\right\rangle}{\langle P(r,\ L)\rangle^2} - 1 \qquad (6)$$

where $P(r, L)$ is being the received power and $\langle\ \rangle$denotes the ensemble average. All results are obtained after curve fitting operation is applied in MATLAB.

3 Numerical results and discussions

In this section of the article, investigations of simulations are reported as follows. Figure 2 and 3 depict the intensity distribution of odd modes on the source plane. In case of

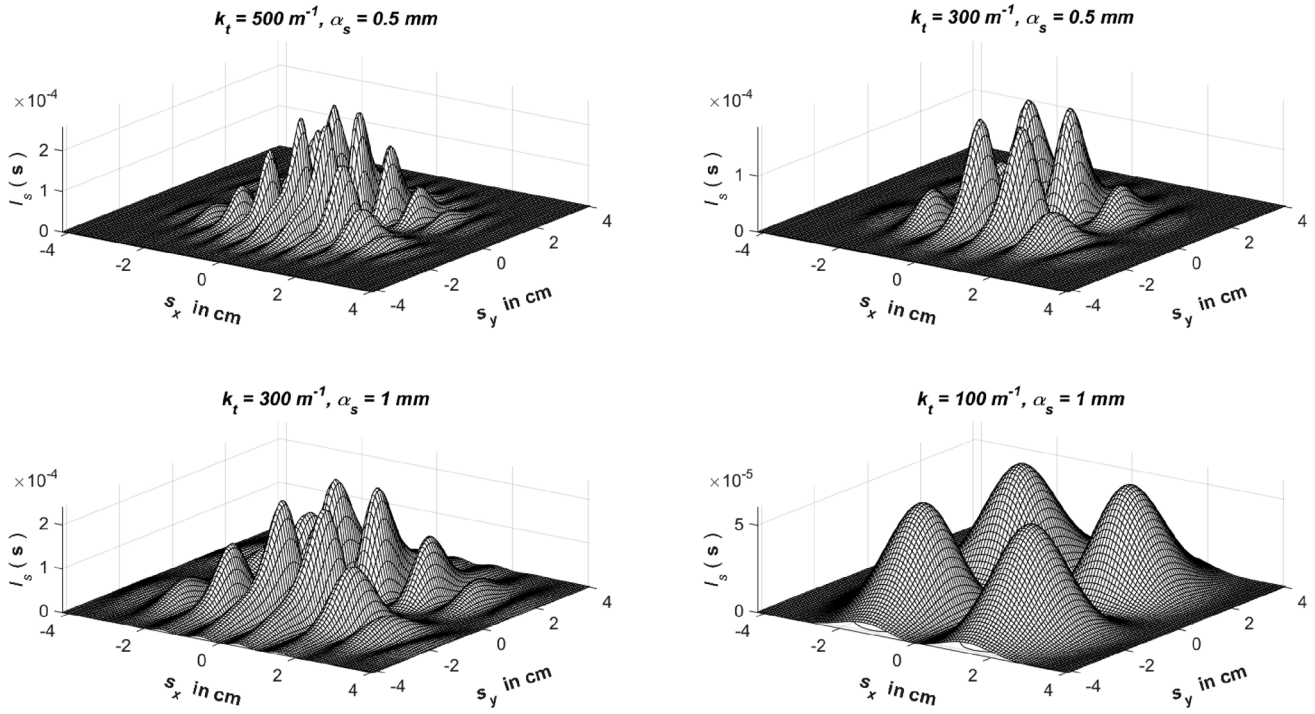

Fig. 2 Intensity distribution of $u_{os_{2n+2}}$

Fig. 3 Intensity distribution of $u_{os_{2n+1}}$

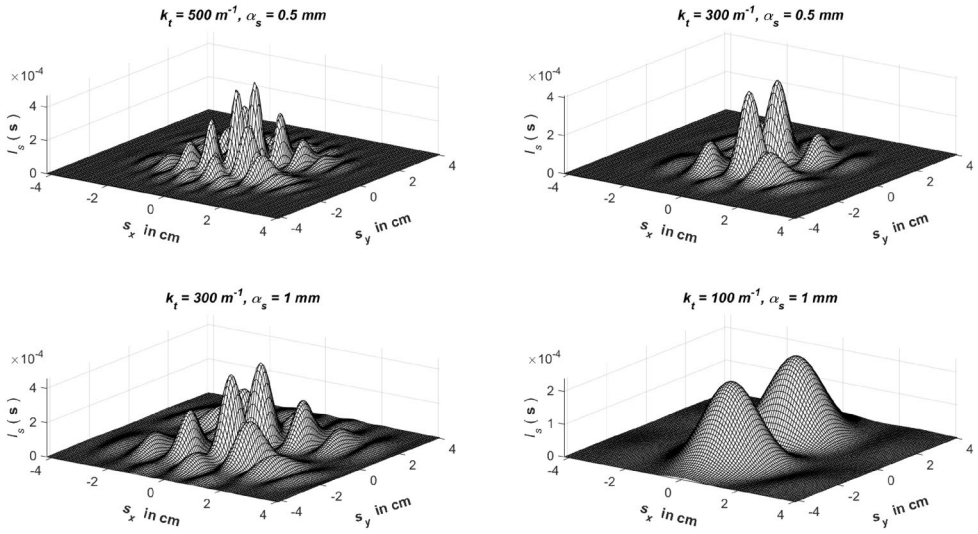

$u_{os_{2n+2}}$, there are four Gaussian lobes symmetrically located on the corners of the source plane if parameters are set as $k_t = 100$ m^{-1} and $\alpha_s = 1$ mm. Additional side lobes with lower intensity are seen with the increase of k_t. These side lobes are added on $x = \pm 3$ cm and lie along y-axis. Beam will be narrower intensity distribution if α_s is decreased. For the parameters $k_t = 500$ m^{-1} and $\alpha_s = 0.5$ mm, totally 6 side lobes (3 of them are on negative × values, 3 of them are on positive × values) are observed in addition to 4 main Gaussian peaks. Intensity distribution of odd mode $u_{os_{2n+1}}$ is shown in Fig. 3. Looking at this figure, two Gaussian peak lying along y-axis is observed for the case of $k_t = 100$ m^{-1} and $\alpha_s = 1$ mm. Idea behind distributions of other subplots is similar with Fig. 2. Furthermore, side lobes are placed symmetrically along xy-axises with the raise of k_t. It is seen 14 side lobes for the beam with k_t parameters $k_t = 300$ m^{-1} and $\alpha_s = 1$ mm. Additional lobes are seen but intensities are mitigated and beam has narrower profile with the reduction of α_s. In case of $k_t = 500$ m^{-1} and $\alpha_s = 0.5$ mm, so many side lobes occur and narrower beam profile attracts the attention. In Fig. 4, we see intensity distribution of $u_{es_{2n}}$ which is the one of the even modes on the source plane. Irregular distribution of this mode leaps to the eye. Despite this untidy shape, we investigate that intensity of side lobes raises with the increase of k_t. On the other hand, decrease in α_s brings the vanishment in side lobes. Among the selected beam types, beam with $k_t = 100$ m^{-1} and $\alpha_s = 1$ mm has the most smooth profile. Intensity distribution of another even mode which is named as $u_{es_{2n+1}}$ on the source plane is presented in Fig. 5. Except beam which $k_t = 100$ m^{-1} and $\alpha_s = 1$ mm, other beams has an intensity distribution looks like sliced Gaussian distribution. Looking at this figure, we investigate that decrease in k_t brings us the beam with less slices. Considering α_s, it is seen that we can have wider beam profile for larger α_s values. In case of $k_t = 100$ m^{-1} and $\alpha_s = 1$ mm, we can see that there is only two Gaussian lobes which are aligned along x-axis. As compared to Fig. 3, Gaussian lobes are placed along x-axis with a rotate of 90°.

On-axis (point like) scintillation of Mathieu–Gauss beams are shown in next six figures. Figure 6 investigates on-axis scintillation of odd Mathieu–Gauss beams when refractive index structure constant $C_n^2 = 10^{-14} m^{-2/3}$. MGB u_{os2n+2} with parameters $k_t = 300$ m^{-1} and $\alpha_s = 0.5$ mm is the worst beam among the selected ones. u_{os2n+1} with $k_t = 500$ m^{-1} and $\alpha_s = 0.5$ mm is nearly the same as spherical wave and u_{os2n+2} with $k_t = 300$ m^{-1} and $\alpha_s = 1$ mm is worse than Gauss beam. u_{os2n+1} with $k_t = 300$ m^{-1} and $\alpha_s = 1$ mm brings no longer advantage since it is nearly the same as Gauss beam. Beams with low k_t and higher α_s values are better than Gauss beam. After 2.5 km distance, $u_{os_{2n+2}}$ with $k_t = 500$ m^{-1} and $\alpha_s = 0.5$ mm and $u_{os_{2n+1}}$ with $k_t = 300$ m^{-1} and $\alpha_s = 0.5$ mm show the best performance for moderate turbulence conditions. With increase in turbulence strength in Fig. 7, beams $u_{os_{2n+2}}$ with $k_t = 300$ m^{-1} and $\alpha_s = 0.5$ mm

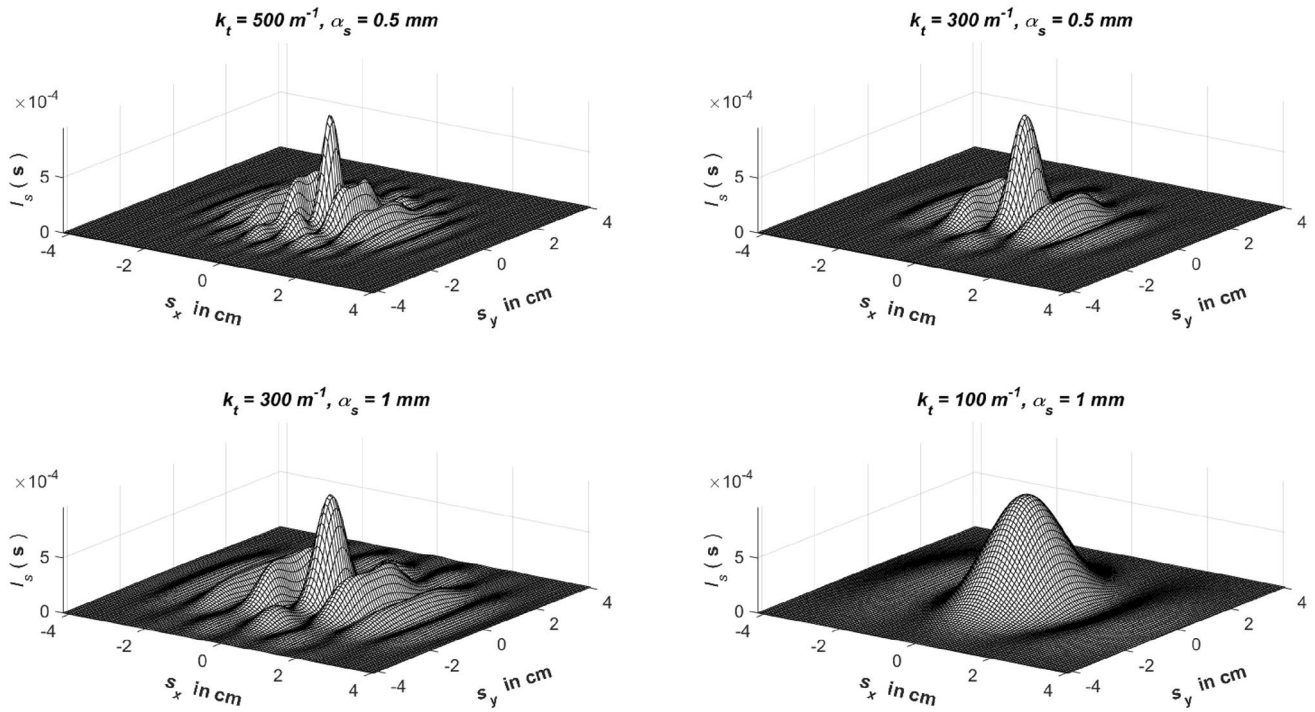

Fig. 4 Intensity distribution of $u_{es_{2n}}$

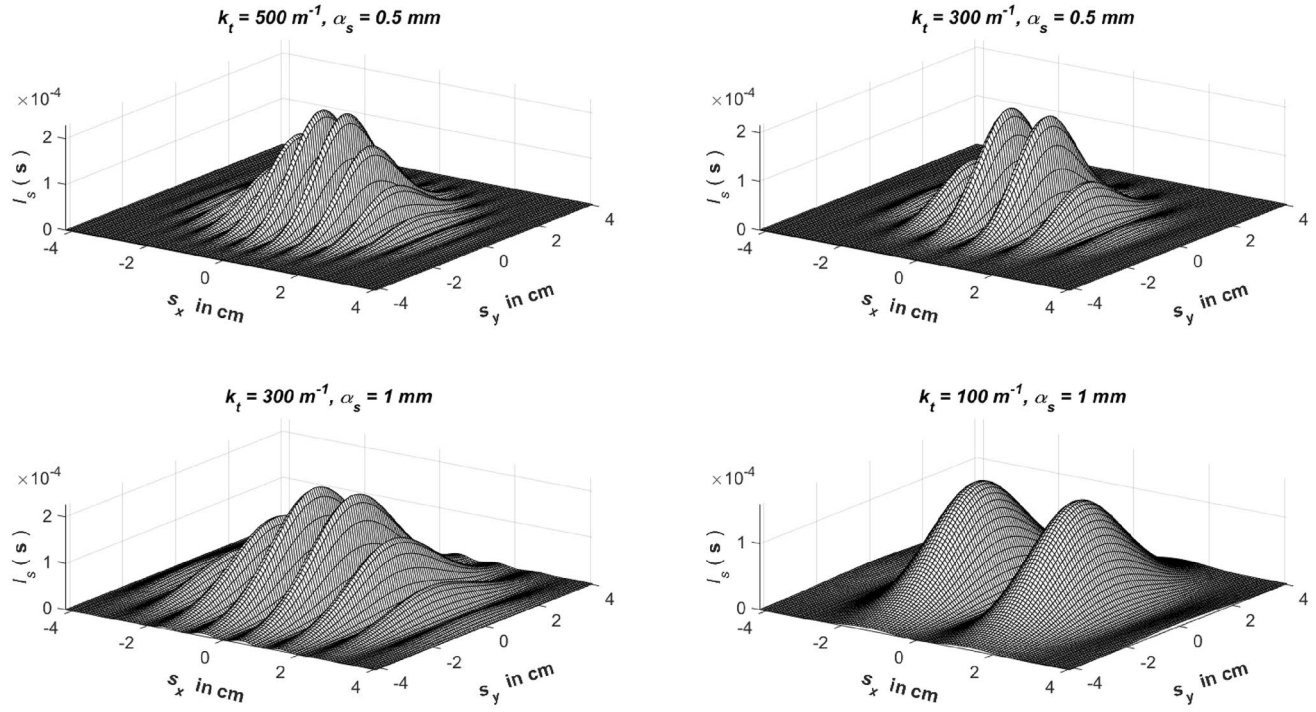

Fig. 5 Intensity distribution of $u_{es_{2n+1}}$

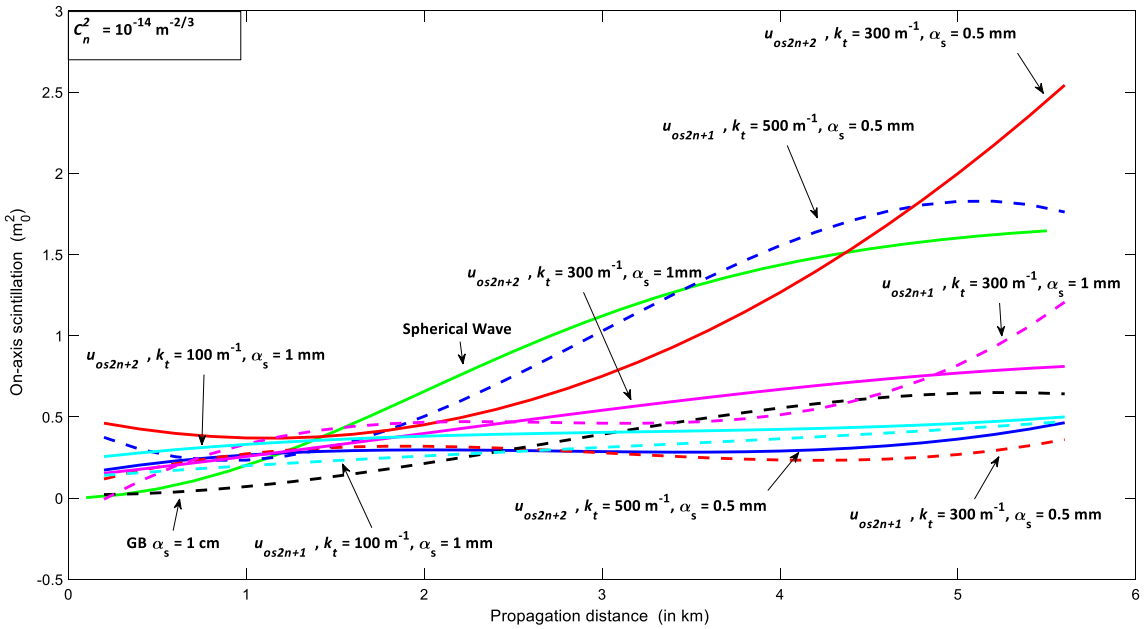

Fig. 6 On-axis scintillation of odd Mathieu–Gauss beams versus propagation distance when $C_n^2 = 10^{-14}$ m$^{-2/3}$

and $u_{os_{2n+2}}$ with $k_t = 300$ m^{-1} and $\alpha_s = 1$ mm have higher scintillation index than spherical wave and Gauss beam. After 1 km up to 5.6 km distance, other odd MGBs show their advantage in case of on-axis scintillation. In this region, $u_{os_{2n+1}}$ with $k_t = 300$ m^{-1} and $\alpha_s = 0.5$ mm and $u_{os_{2n+1}}$ with $k_t = 300$ m^{-1} and $\alpha_s = 1$ mm have the least scintillation index. $u_{os_{2n+1}}$ with $k_t = 100$ m^{-1} and $\alpha_s = 1$ mm and $u_{os_{2n+2}}$ with $k_t = 100$ m^{-1} and $\alpha_s = 1$ mm are also advantageous comparing with commercial laser output Gauss beam. While odd MGB $u_{os_{2n+2}}$ with $k_t = 500$ m^{-1} and $\alpha_s = 0.5$ mm seems

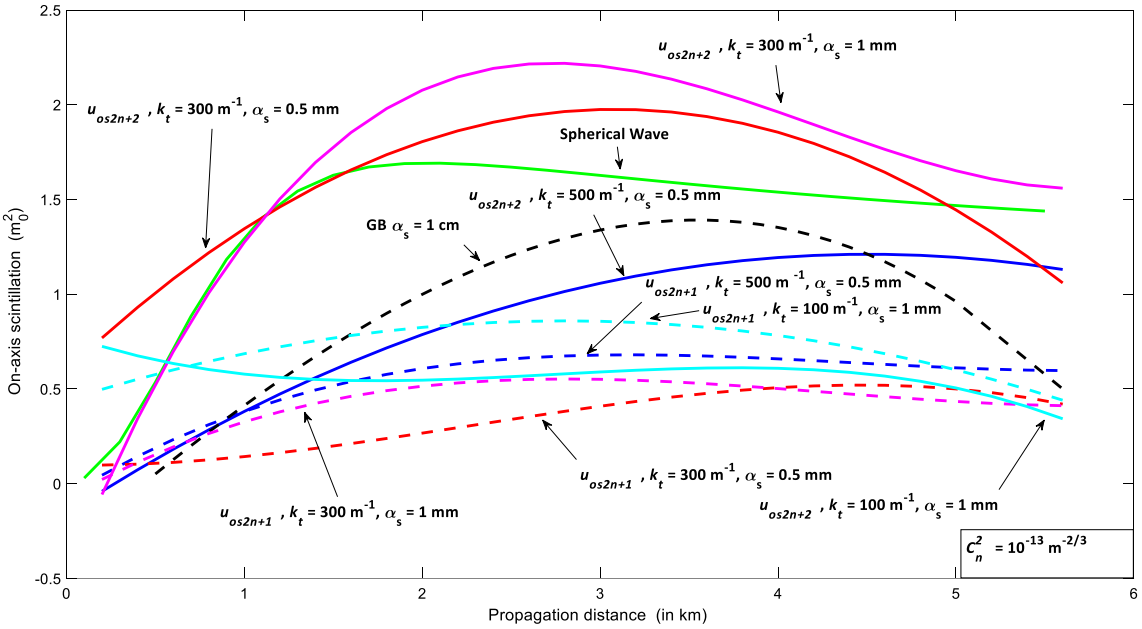

Fig. 7 On-axis scintillation of odd Mathieu–Gauss beams versus propagation distance when $C_n^2 = 10^{-13}$ m$^{-2/3}$

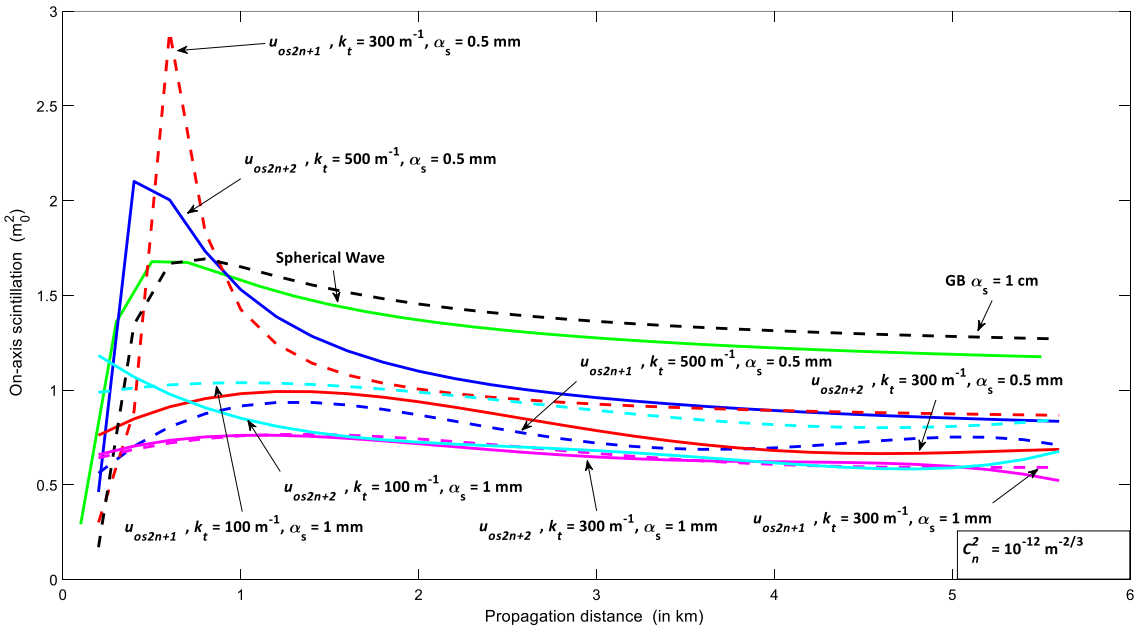

Fig. 8 On-axis scintillation of odd Mathieu–Gauss beams versus propagation distance when $C_n^2 = 10^{-12}$ m$^{-2/3}$

advantageous for the same region, $u_{os_{2n+2}}$ with $k_t = 500$ m^{-1} and $\alpha_s = 0.5$ mm loses its advantage in 4.5 km distance. Figure 8 shows on-axis scintillation under strong turbulence conditions. Looking at this figure, we see that all selected MGBs have less scintillation index than Gauss beam and spherical wave after 1 km distance. Because, both $u_{os_{2n+2}}$ with $k_t = 500$ m^{-1} and $\alpha_s = 0.5$ mm and $u_{os_{2n+1}}$ with $k_t = 300$ m^{-1} and $\alpha_s = 0.5$ mm have the highest scintillation index between 0.5-1 km distance. After this propagation distance, they provide the advantage against Gauss beam. In this case, $u_{os_{2n+2}}$ with $k_t = 300$ m^{-1} and $\alpha_s = 0.5$ mm is the worst of MGBs but still better than Gauss beam. $u_{os_{2n+2}}$ with $k_t = 500$ m^{-1} and $\alpha_s = 0.5$ mm is also close to the worst one. $u_{os_{2n+2}}$ with $k_t = 300$ m^{-1} and $\alpha_s = 1$ mm, $u_{os_{2n+1}}$ with $k_t = 300$ m^{-1} and

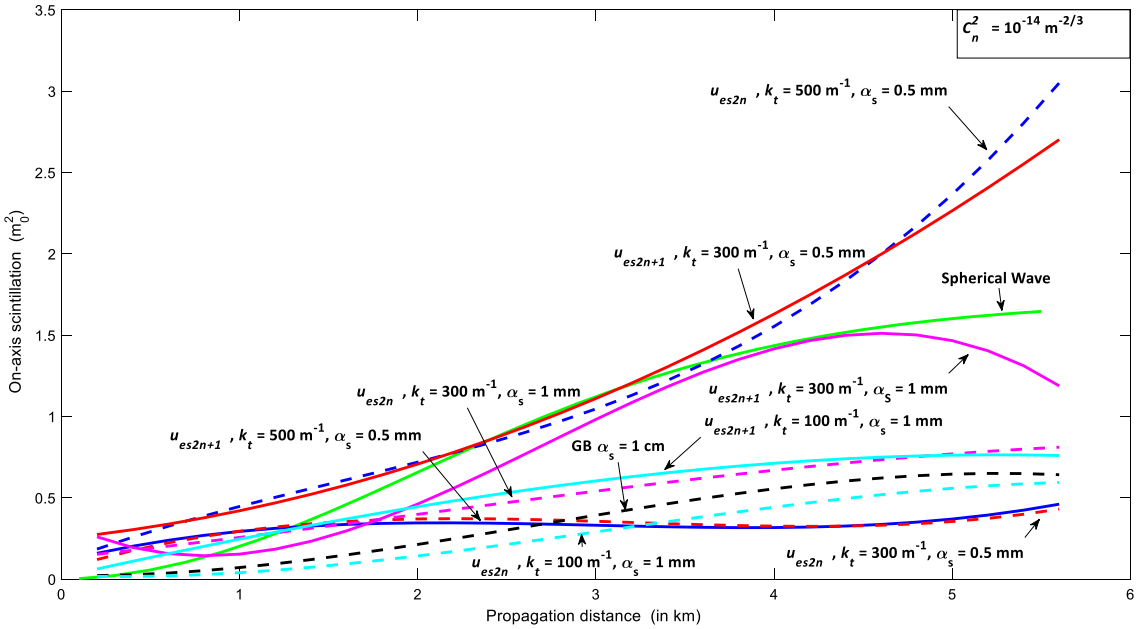

Fig. 9 On-axis scintillation of even Mathieu–Gauss beams versus propagation distance when $C_n^2 = 10^{-14}$ m$^{-2/3}$

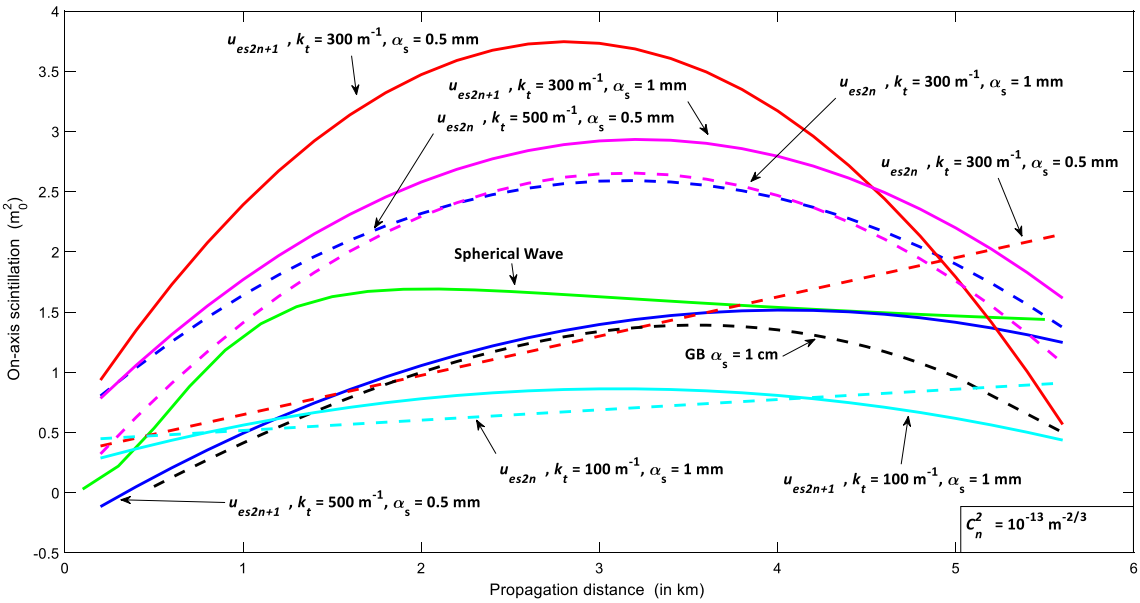

Fig. 10 On-axis scintillation of even Mathieu–Gauss beams versus propagation distance when $C_n^2 = 10^{-13}$ m$^{-2/3}$

$\alpha_s = 1$ mm, $u_{os_{2n+2}}$ with $k_t = 100$ m^{-1} and $\alpha_s = 1$ mm and has the least scintillation index among the selected beams. Remaining MGBs are located between the better and worse ones.

In the analysis of even modes of MGB, Figs. 9, 10, and 11 are plotted under turbulence conditions from $C_n^2 = 10^{-14}m^{-2/3}$ to $C_n^2 = 10^{-12}m^{-2/3}$. In Fig. 9, u_{es} with $k_t = 300$ m^{-1} and $\alpha_s = 0.5$ mm and $u_{es_{2n+1}}$ with $k_t = 500$ m^{-1} and $\alpha_s = 0.5$ mm have the least scintillation index than Gauss beam for more than 2.5 km distance. $u_{es_{2n+1}}$ with $k_t = 100$ m^{-1} and $\alpha_s = 1$ mm is also advantageous with a slight difference in the same distance. $u_{es_{2n}}$ with $k_t = 100$ m^{-1} and $\alpha_s = 1$ mm and $u_{es_{2n}}$ with $k_t = 300$ cm^{-1} and $\alpha_s = 1$ mm are close to each other and have higher scintillation index than Gauss beam. $u_{es_{2n+1}}$ with $k_t = 300$ m^{-1} and $\alpha_s = 1$ mm shows similar performance with spherical

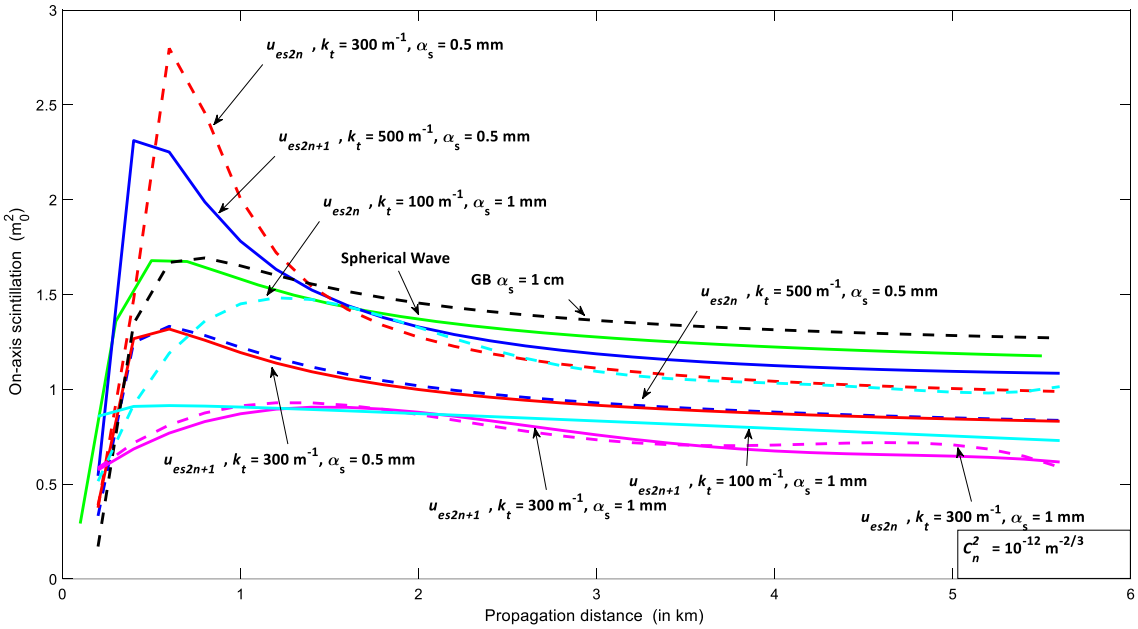

Fig. 11 On-axis scintillation of even Mathieu–Gauss beams versus propagation distance when $C_n^2 = 10^{-12}$ m$^{-2/3}$

wave.$u_{es_{2n}}$ with $k_t = 500$ m^{-1} and $\alpha_s = 0.5$ mm and $u_{es_{2n+1}}$ with $k_t = 300$ m^{-1} and $\alpha_s = 0.5$ mm have the highest scintillation index in moderate turbulence settings. Figure 10 depicts on-axis scintillation index when $C_n^2 = 10^{-13} m^{-2/3}$. Looking at this figure, we investigate that both modes of $k_t = 100$ m^{-1} and $\alpha_s = 1$ mm have the least scintillation index after 2 km distance. However, $u_{es_{2n}}$ with $k_t = 300$ m^{-1} and $\alpha_s = 0.5$ mm has higher scintillation index than Gauss beam. Additionally, $u_{es_{2n+1}}$ with $k_t = 500$ m^{-1} and $\alpha_s = 0.5$ mm has less scintillation index than Gauss beam only between 0.75 and 2.5 km distance. Remaining settings of MGB have higher scintillation index than Gauss beam and spherical wave. Beams can be listed from the highest index to lowest one as $u_{es_{2n+1}}$ with $k_t = 300$ m^{-1} and $\alpha_s = 0.5$ mm, $u_{es_{2n+1}}$ with $k_t = 300$ m^{-1} and $\alpha_s = 1$ mm, $u_{es_{2n}}$ with $k_t = 500$ m^{-1} and $\alpha_s = 0.5$ mm, and $u_{es_{2n}}$ with $k_t = 300$ m^{-1} and $\alpha_s = 1$ mm. $u_{es_{2n+1}}$ with $k_t = 500$ m^{-1} and $\alpha_s = 0.5$ mm and $u_{es_{2n}}$ with $k_t = 300$ m^{-1} and $\alpha_s = 0.5$ mm have similar behavior with Gauss beam. Scintillation index of $u_{es_{2n+1}}$ with $k_t = 300$ m^{-1} and $\alpha_s = 0.5$ mm sharply decreases and trend shows that it is the best one in longer distances. Looking at Fig. 11, we can say that similar with odd modes, all settings of MGB have less scintillation index than Gauss beam and spherical wave for strong turbulence conditions after 1.5 km distance. Although, beams $u_{es_{2n}}$ with $k_t = 300$ m^{-1} and $\alpha_s = 0.5$ mm and $u_{es_{2n+1}}$ with $k_t = 500$ m^{-1} and $\alpha_s = 0.5$ mm have the highest scintillation index in closer distances, their scintillation index falls below the ones of Gauss beam and spherical wave. Both types of $k_t = 300$ m^{-1} and $\alpha_s = 0.5$ mm take the lead in this condition. Next, $u_{es_{2n+1}}$ with $k_t = 300$ m^{-1} and $\alpha_s = 0.5$ mm,$u_{es_{2n+1}}$ with $k_t = 300$ m^{-1} and $\alpha_s = 0.5$ mm, and u_{es2n} with $k_t = 500$ m^{-1} and $\alpha_s = 0.5$ mm follow them with slight difference. u_{es2n} with $k_t = 100$ m^{-1} and $\alpha_s = 1$ mm is close to MGB with u_{es2n} with $k_t = 300$ m^{-1} and $\alpha_s = 0.5$ mm.

In addition to above investigations, on-axis scintillation index of odd MGB is generally less than even modes for weak turbulent conditions. Under strong turbulent regimes, odd modes have generally less scintillation index than even modes for close distances. On the other hand, odd modes and even modes are nearly the same for longer distances. We deduce from these figures that MGB having less complicated intensity distribution on the source plane have less scintillation index. Additional side lobes cause to raise in scintillation index. Furthermore, scintillation index of wider beams is less as compared to small beams. As it is mentioned in source size in (Andrews 2005) an interval reduces both outer scale effect and scintillation. As usual, beams generally have rising trend in weak turbulent region, decaying behavior in moderate turbulence, and saturated trend in strong turbulence.

Figures 12 and 13 examine the aperture averaging effect on odd and even modes of MGBs respectively when $C_n^2 = 10^{-12} m^{-2/3}$. Looking at Fig. 12, we first emphasize that advantage in terms of aperture average scintillation decreases with the increase in receiver aperture radius. Furthermore, all selected odd MGBs have less aperture averaged scintillation than Gauss beam. More specifically, both types of $k_t = 300$ m^{-1} and $\alpha_s = 1$ mm have the least scintillation index for all aperture radius. Next,

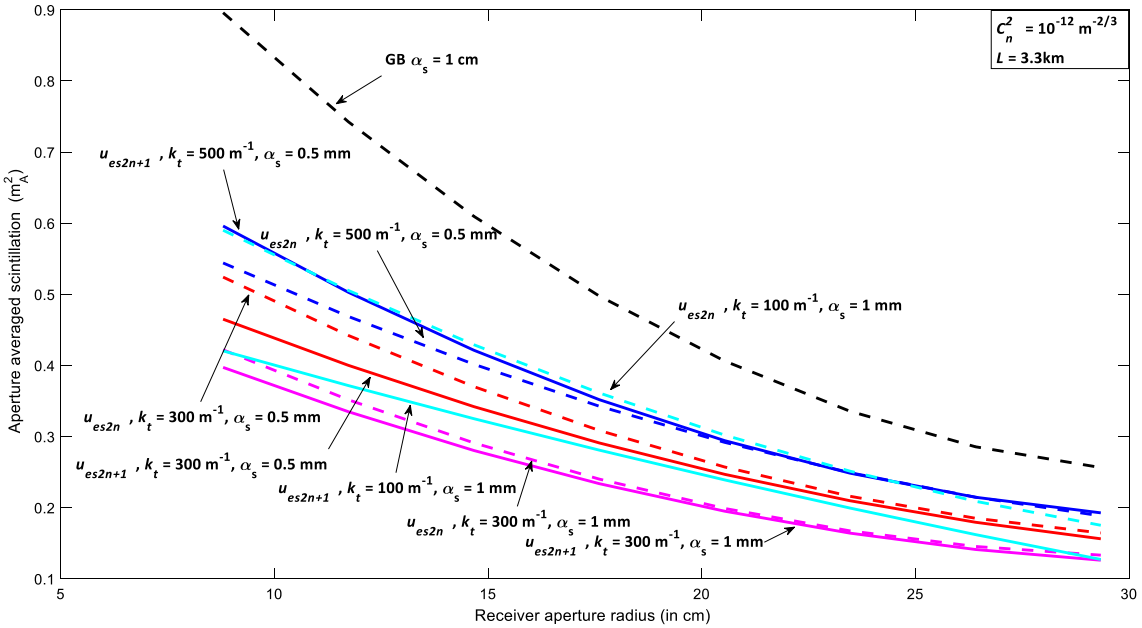

Fig. 12 Aperture averaged scintillation of odd Mathieu–Gauss beam against receiver aperture opening when $C_n^2 = 10^{-12}$ m$^{-2/3}$

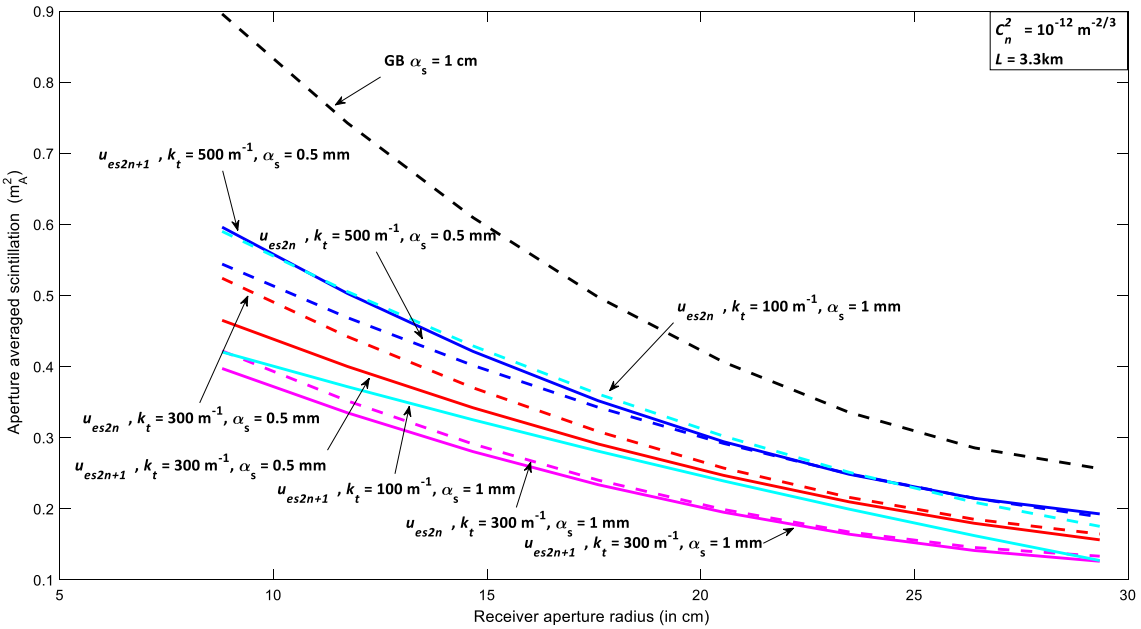

Fig. 13 Aperture averaged scintillation of even Mathieu–Gauss beam against receiver aperture opening when $C_n^2 = 10^{-12}$ m$^{-2/3}$

$u_{os_{2n+2}}$ with $k_t = 100$ m^{-1} and $\alpha_s = 1$ mm follows them. Both $k_t = 300$ m^{-1} and $\alpha_s = 0.5$ mm is placed in the middle of MGBs but $u_{os_{2n+2}}$ have a slight advantage. $U_{os_{2n+1}}$ with $k_t = 500$ m^{-1} and $\alpha_s = 0.5$ mm shows moderate performance in smaller aperture openings on the other hand other settings show worse performance for larger apertures. Other type of $k_t = 500$ m^{-1} and $\alpha_s = 0.5$ mm is generally the worst of MGBs but it is still better than Gauss beam. Finally, $u_{os_{2n+1}}$ with $k_t = 100$ m^{-1} and $\alpha_s = 1$ mm takes place in the middle of MGBs while it is the worst in smaller apertures. In the analysis of aperture averaged scintillation of even MGBs, all settings show better performance than Gauss beam. Similar with odd MGBs, beams with $k_t = 500$ m^{-1} and $\alpha_s = 0.5$ mm have the highest scintillation index for

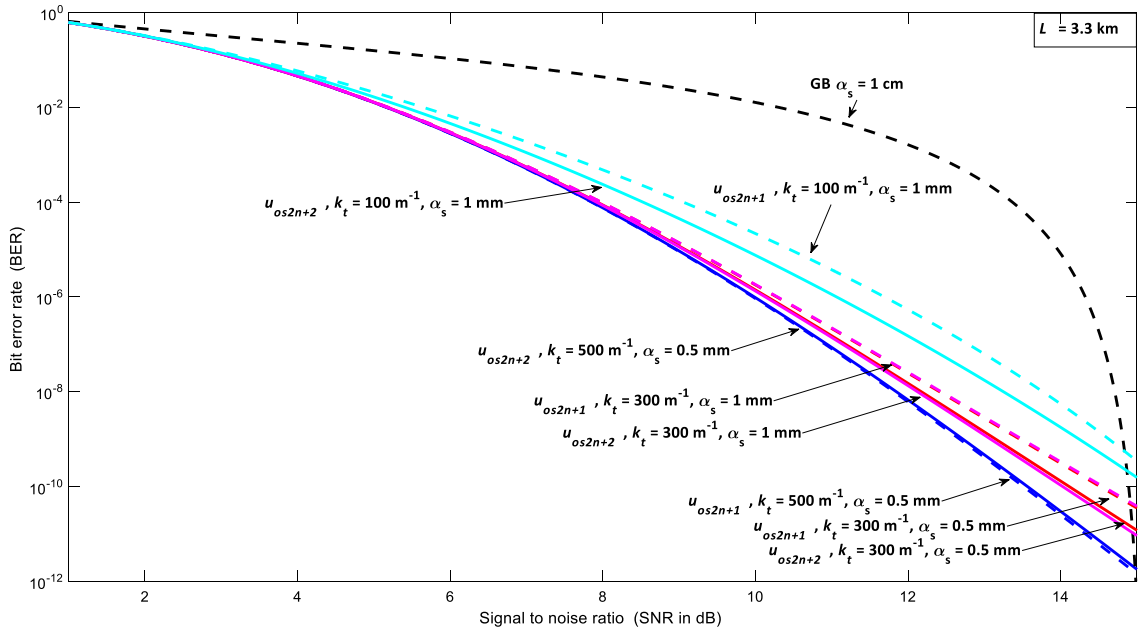

Fig. 14 Bit error rate behavior of odd Mathieu beams against SNR

both small and large aperture openings. Again similar with previous figure, $u_{es_{2n}}$ with $k_t = 100$ m^{-1} and $\alpha_s = 1$ mm is close to beams with large k_t value. As opposed to them, both versions of $k_t = 300$ m^{-1} and $\alpha_s = 1$ mm have the least scintillation index. In addition, $u_{es_{2n+1}}$ with $k_t = 100$ m^{-1} and $\alpha_s = 1$ mm and both types of $k_t = 300$ m^{-1} and $\alpha_s = 0.5$ mm is placed in between the best and worst even MGBs.

Figure 14 shows bit error rate performance of odd MGB against signal to noise ratio. All settings of MGBs show better performance in the interval of [0,15 dB], even though they lose their advantage after this value. From the best one to the worst of odd MGBs, beams can be listed as $u_{os_{2n+1}}$ with $k_t = 500$ m^{-1} and $\alpha_s = 0.5$ mm, $u_{os_{2n+2}}$ with $k_t = 500$ m^{-1} and $\alpha_s = 0.5$ mm, $u_{os_{2n+2}}$ with $k_t = 300$ m^{-1} and $\alpha_s = 1$ mm, $u_{os_{2n+2}}$

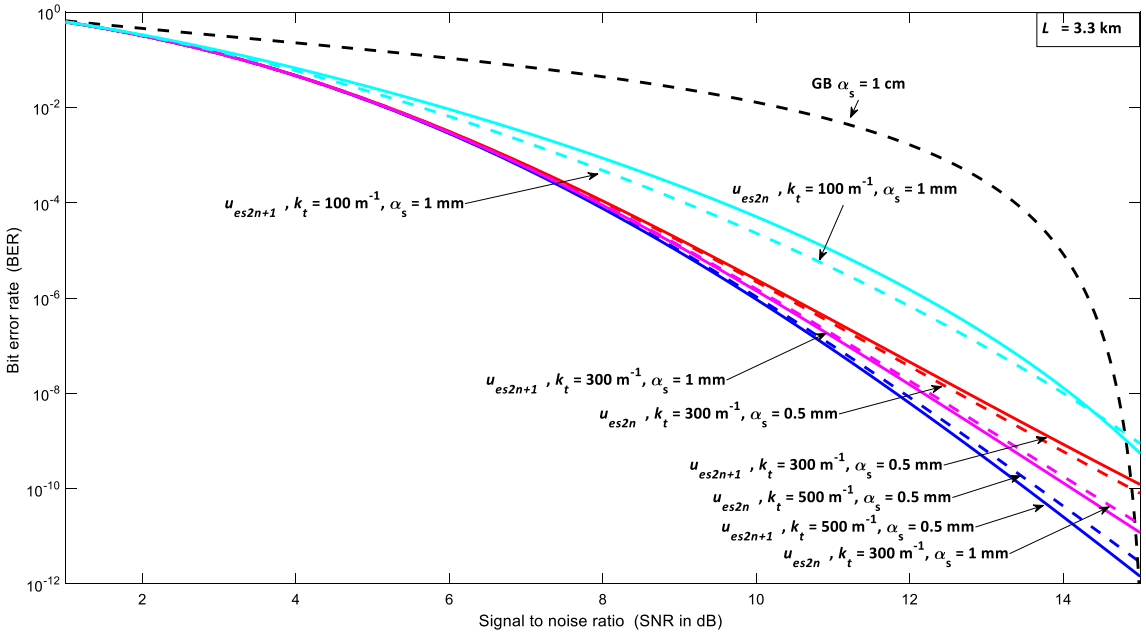

Fig. 15 Bit error rate behavior of even Mathieu beams against SNR

with $k_t = 300\ \mathrm{m}^{-1}$ and $\alpha_s = 0.5$ mm, $u_{os_{2n+1}}$ with $k_t = 300\ \mathrm{m}^{-1}$ and $\alpha_s = 0.5$ mm, $u_{os_{2n+1}}$ with $k_t = 300\ \mathrm{m}^{-1}$ and $\alpha_s = 1$ mm, $u_{os_{2n+2}}$ with $k_t = 100\ \mathrm{m}^{-1}$ and $\alpha_s = 1$ mm, and $u_{os_{2n+1}}$ with $k_t = 100\ \mathrm{m}^{-1}$ and $\alpha_s = 1$ mm. It is clear to see that odd modes of MGBs bring 10^{-4} to 10^{-6} times lower BER in optical wireless communication systems. Last figure shows BER performance of even modes of MGBs. Similarly, even MGBs are advantageous up to 15 dB SNR. In this case, the lowest BER value belongs to $u_{es_{2n+1}}$ with $k_t = 500\ \mathrm{m}^{-1}$ and $\alpha_s = 0.5$ mm. Then, its $u_{es_{2n}}$ version follows it. Next, $u_{es_{2n+1}}$ with $k_t = 300\ \mathrm{m}^{-1}$ and $\alpha_s = 1$ mm and its $u_{es_{2n}}$ version take place. $u_{es_{2n}}$ with $k_t = 300\ \mathrm{m}^{-1}$ and $\alpha_s = 0.5$ mm and $u_{es_{2n+1}}$ with the same parameters have higher BER than $k_t = 300\ \mathrm{m}^{-1}$ and $\alpha_s = 1$ mm couple. Finally, $u_{es_{2n}}$ with small k_t and higher α_s value and its $u_{es_{2n+1}}$ type have the highest BER among MGBs. As a summary of our investigations about BER performance of even modes, usage of even modes mitigates BER value approximately 10^{-3} to $10^{-5.5}$ times comparing with Gauss beam (Fig. 15).

4 Conclusion

On-axis, aperture averaged scintillation, and bit error rate of Mathieu–Gauss beams is studied in this paper. In addition to studies in literature, number of screens in RPS is increased to cover the strong turbulent regime. Even though turbulence strength increases, scintillation index of odd and even modes of MGBs is less as compared to Gauss beam and spherical wave. In the comparison of odd and even modes, odd modes attract the attention with its less scintillation index. Effect of low scintillation index reflects on bit error rate. While even modes of MGBs provide $10^{-5.5}$ times lesser bit error rate than Gauss beam, BER can be mitigated 10^{-6} times less with usage of odd modes. We hope that our results will be beneficial for current free space optics design processes.

References

Alvarez-Elizondo MB, Rodriguez-Masegosa R, Gutierrez-Vega JC (2008) Generation of Mathieu–Gauss modes with an axicon-based laser resonator. Opt Express 16:18770–18775

Andrews LC (2005) Laser beam propagation through random media. SPIE, Washington

Andrews LC, Philips RL (2004) Free space optical communication link and atmospheric effects: single aperture and arrays. In: Free-space laser communication technologies XVI. https://doi.org/10.1117/12.556737

Andrews LC, Al-Habash MA, Hopen CY, Phillips RL (2001) Theory of optical scintillation: Gaussian-beam wave model. Wave Random Complex 11:271–291

Arpali SA, Eyyuboglu HT, Baykal Y (2008) Bit error rates for general beams. Appl Opt 47:5971–5975

Bandres MA, Gutierrez-Vega JC, Chavez-Cerda S (2004) Parabolic nondiffracting optical wave fields. Opt Lett 29:44–46

Barcelo-Chong A, Estrada-Portillo B, Canales-Benavides A, Lopez-Aguayo S (2018) Asymmetric Mathieu beams. Chin Opt Lett 16:122601

Baykal Y, Eyyuboğlu HT, Cai Y (2008) Incoherent sinusoidal-Gaussian and annular beam scintillations. In: Fourteenth international symposium on atmospheric and ocean optics/atmospheric physics, pp 69360B

Bayraktar M (2019) Estimation of scintillation and bit error rate performance of sine hollow beam via random phase screen. Optik 188:147–154

Bayraktar M, Eyyuboglu HT (2019) Propagation properties of optical bottle beam in turbulence. Opt Eng 58:036104

Chafiq A, Hricha Z, Belafhal A (2006) A detailed study of Mathieu–Gauss beams propagation through an apertured ABCD optical system. Opt Commun 265:594–602

Durnin J, Miceli JJ, Eberly JH (1987) Diffraction-free beams. Phys Rev Lett 59:2612

Eyyuboglu HT (2013a) Estimation of aperture averaged scintillations in weak turbulence regime for annular, sinusoidal and hyperbolic Gaussian beams using random phase screen. Opt Laser Technol 52:96–102

Eyyuboglu HT (2013b) Scintillation analysis of hypergeometric Gaussian beam via phase screen method. Opt Commun 309:103–107

Eyyuboglu HT (2013c) Scintillation behavior of Airy beam. Opt Laser Technol 47:232–236

Eyyuboglu HT (2015a) Apertured averaged scintillation of fully and partially coherent Gaussian, annular Gaussian, flat toped and dark hollow beams. Opt Commun 339:141–147

Eyyuboglu HT (2015b) Per unit received power apertured averaged scintillation of partially coherent sinusoidal and hyperbolic Gaussian beams. Opt Laser Technol 71:55–62

Eyyuboglu HT, Bayraktar M (2015) SNR bounds of FSO links and its evaluation for selected beams. J Mod Opt 62:1316–1322

Fried DL, Seidman JB (1967) Laser beam scintillation in the atmosphere. J Opt Soc Am 57:181–185

Gercekcioglu H, Baykal Y (2013) BER of annular and flat-topped beams in non-Kolmogorov weak turbulence. Opt Commun 286:30–33

Gercekcioglu H, Baykal Y (2014) Scintillation and BER for optimum sinusoidal Gaussian beams in weak non-Kolmogorov turbulence. Opt Commun 320:1–5

Gerçekçioğlu H, Baykal Y, Eyyuboğlu HT (2010) BER of annular beams in strong turbulence. In: Applications of lasers for sensing and free space communications 2010, paper LSTuA4

Gradshteyn IS, Ryzhik IM (2015) Table of integrals, series, and products. Academic Press, Amsterdam

Gutierrez-Vega JC, Bandres MA (2007) Normalization of the Mathieu–Gauss optical beams. J Opt Soc Am A 24:215–220

Gutierrez-Vega JC, Iturbe-Castillo MD, Chavez-Cerda S (2000) Alternative formulation for invariant optical fields: Mathieu beams. Opt Lett 25:1493–1495

Gutierrez-Vega JC, Iturbe-Castillo MD, Ramirez GA, Tepichin E, Rodriguez-Dagnino RM, Chavez-Cerda S, New GHC (2001) Experimental demonstration of optical Mathieu beams. Opt Commun 195:35–40

Gutiérrez-Vega JC, Iturbe-Castillo MD, Tepichin E, Ramírez G, Rodríguez-Dagnino RM, Chávez-Cerda S (2000) New member in the family of propagation-invariant optical fields: Mathieu beams. Opt Photonics News 11:37–38

Hernandez-Aranda RI, Gutierrez-Vega JC, Guizar-Sicairos M, Bandres MA (2006) Propagation of generalized vector Helmholtz-Gauss beams through paraxial optical systems. Opt Express 14:8974–8988

Hernandez-Hernandez RJ, Terborg RA, Ricardez-Vargas I, Volke-Sepulveda K (2010) Experimental generation of Mathieu–Gauss beams with a phase-only spatial light modulator. Appl Opt 49:6903–6909

Li HR, Yin JP (2011) Generation of a vectorial Mathieu-like hollow beam with a periodically rotated polarization property. Opt Lett 36:1755–1757

Lopez-Mariscal C, Gutierrez-Vega JC, Milne G, Dholakia K (2006) Orbital angular momentum transfer in helical Mathieu beams. Opt Express 14:4182–4187

Noriega-Manez RJ, Gutierrez-Vega JC (2007) Rytov theory for Helmholtz-Gauss beams in turbulent atmosphere. Opt Express 15:16328–16341

Öztan MA, Baykal Y (2010) Scintillation index of partially coherent asymmetrical multi Gaussian beams in extremely strong turbulence. In: National conference on electrical, electronics and computer engineering, pp 433–437

Priyalakshmi B, Mahalakshmi K (2020) Performance analysis of video transmission in vertical-UWOC link in mid-sea oil rig IoT systems. J Ambient Intell Human Comput. https://doi.org/10.1007/s12652-020-02081-0

Qian XM, Zhu WY, Rao RZ (2009) Numerical investigation on propagation effects of pseudo-partially coherent Gaussian Schell-model beams in atmospheric turbulence. Opt Express 17:3782–3791

Rao RZ (2008) Statistics of the fractal structure and phase singularity of a plane light wave propagation in atmospheric turbulence. Appl Opt 47:269–276

Ren ZJ, Hu HH, Peng BJ (2018) Generation of Mathieu beams using the method of 'combined axicon and amplitude modulation'. Opt Commun 426:226–230

Schmidt JD (2010) Numerical simulation optical wave propagation with examples in MATLAB. SPIE, Washington

Sumathi K, Balasaraswathi M, Boopathi CS, Singh M, Malhotra J, Dhasarathan V (2020) Design of 3.84 Tbps hybrid WDM–PDM based inter-satellite optical wireless communication (IsOWC) system using spectral efficient orthogonal modulation scheme. J Ambient Intell Human Comput. https://doi.org/10.1007/s12652-020-01691-y

Yao M (2009) Scintillation index of astigmatic annular beams in a turbulent atmosphere. Optik 120:824–828

Zhang YL, Ma DL, Zhou ZY, Yuan XH (2017) Research on partially coherent flat-topped vortex hollow beam propagation in turbulent atmosphere. Appl Opt 56:2922–2926